American Mineralogist, Volume 96, pages 744–751, 2011

First-principles study of diffusion and viscosity of anorthite ($CaAl_2Si_2O_8$) liquid at high pressure

Bijaya B. Karki,[1,2,*] Bidur Bohara,[1] and Lars Stixrude[3]

[1]Department of Computer Science, Louisiana State University, Baton Rouge, Louisiana 70803, U.S.A.
[2]Department of Geology and Geophysics, Louisiana State University, Baton Rouge, Louisiana 70803, U.S.A.
[3]Department of Earth Sciences, University College London, London WC1E 6BT, U.K.

Abstract

We have carried out equilibrium molecular dynamics simulations of $CaAl_2Si_2O_8$ (anorthite) liquid as a function of pressure (up to 160 GPa) and temperature (2500 to 6000 K) within density functional theory. Along the 3000 K isotherm, the Ca self-diffusivity varies most (decreasing by two orders of magnitude between 0 and 50 GPa), whereas the self-diffusion coefficients of Al, Si, and O vary anomalously—they initially increase with pressure, reach the broad maxima (around 5 GPa), and then decrease upon further compression. The calculated melt viscosity also shows a weak anomalous behavior with a local minimum around a similar pressure. Temperature suppresses the dynamical anomalies as well as the overall pressure variations. Therefore, the curvatures of the diffusivity (viscosity) isotherms change from a concave (convex) shape at 3000 K to a convex (concave) shape at 6000 K. We find that anorthite liquid is much more mobile than silica liquid because of its high content of non-bridging oxygen atoms (NBO) and oxygen triclusters (O3). The predicted pressure variations can be associated with structural changes consisting of the pressure-induced maximum in the abundance of pentahedral states (fivefold Al/Si-O coordination) and rapid increase in the O3 abundance. Finally, our predicted first-principles results compare favorably with the available experimental data.

Keywords: Anorthite liquid, diffusion, viscosity, first-principles simulations, high pressure

Introduction

Knowledge about molten silicates is crucial for our understanding of the cooling and crystallization of Earth's early magma ocean as well as for our understanding of present day mantle dynamics (e.g., Rigden et al. 1984; Solomatov 2007). The analysis of xenoliths (e.g., Haggerty and Sautter 1990) and seismic observations (Revenaugh and Sipkin 1994; Lay et al. 2004) suggest that melts can exist at various depths in the mantle including the core-mantle boundary and can have a broad range of composition. In recent years, we have carried out first-principles simulations of melts in the MgO-SiO_2 (binary) system at high pressure and temperature to study their structural and dynamical properties (e.g., Stixrude and Karki 2005; Karki et al. 2006, 2007, 2010; de Koker et al. 2008) including viscosity (Karki and Stixrude 2010a, 2010b).

We chose to study anorthite ($CaAl_2Si_2O_8$) liquid for several reasons: First, it represents a composition in ternary (CaO-Al_2O_3-SiO_2) system. Naturally occurring melts are indeed multi-component silicates. Second, it is considered as a highly polymerized liquid. Such melts are known to show the non-Arrhenian dependence on temperature and also anomalous increase (decrease) of diffusivity (viscosity) with pressure (Bottinga and Richet 1995; Giordano and Dingwell 2003; Tinker et al. 2003, 2004). Third, amorphous anorthite, particularly, in glass form has widely been studied experimentally. Since the experimental measurements are confined to relatively low pressures (Urbain et al. 1982; Taniguchi 1992), to apply these results for the deep mantle requires long extrapolations. In addition, the ways in which the microscopic (atomic) characteristics control the macroscopic (bulk) properties is still an unsolved issue. Fourth, previous computational studies were based mostly on semi-empirical force fields (Nevins and Spera 1998; Morgan and Spera 2001a, 2001b; Winkler et al. 2004; Spera et al. 2009). A first-principle approach based on quantum mechanical formulation has been recently applied to anorthite liquid, with the main focus on the structure and thermodynamics (de Koker 2010).

In this paper, we report equilibrium molecular dynamics (MD) simulations of molten $CaAl_2Si_2O_8$ to study from first-principles diffusion and viscosity as a function of pressure (up to 160 GPa) and temperature (2500 to 6000 K). First, we introduce the methodology in the context of simulations, and derivation and analysis of dynamical properties. Then, we present the specific results and discussion on the equation of state, self-diffusivities, and viscosity of the melt.

Methodology

The first-principles molecular dynamics method, Vienna ab initio simulation package (VASP) (Kresse and Furthmuller 1996), was used within the local density approximation (Ceperley and Alder 1980). The projector augmented wave (PAW) method (Kresse and Joubert 1999) was used with a plane wave cutoff of 400 eV and γ point. Simulations based on the canonical (*NVT*) ensemble were performed

* E-mail: karki@csc.lsu.edu

to explore compression from V/V_X = 1.33 to 0.45 covering pressure range of 0 to 160 GPa at 2500 to 6000 K, where V_X = 3026.23 Å^3 is equal, for the number of atoms (16 $CaAl_2Si_2O_8$ units, i.e., 208 atoms) in our simulation cell, to the reference volume for the self-consistently derived equation of state for anorthite liquid (Ghiorso 2004). The initial structure at each volume was first melted at 6000 K, and then cooled isochorically to lower temperatures. Long simulation durations ranging from 1 to 100 ps with time step (1 fs) were performed to achieve an acceptable convergence. Pressure corrections were included as before (e.g., Karki et al. 2010) with Pulay stress of 2.5 to 7.5 GPa over the volume range studied and an empirical correction of 1.8 GPa applied at each volume.

We compute the self-diffusion coefficient for each species, α, from first-principles equilibrium molecular dynamics simulations using the Einstein relation

$$D_\alpha = \lim_{t\to\infty} \frac{1}{6t} \left\langle \frac{1}{N_\alpha} \sum_{i=1}^{N_\alpha} \left| r_{\alpha,i}(t+t_0) - r_{\alpha,i}(t_0) \right|^2 \right\rangle \quad (1)$$

The positions of the i^{th} atom of type α at time origin t_0 and then after time t are $r_{\alpha,i}(t_0)$ and $r_{\alpha,i}(t + t_0)$, respectively. We calculate the shear viscosity (η) using the Green-Kubo relation

$$\eta = \frac{V}{10 k_B T} \int_0^\infty \left\langle \sum_{\alpha\beta} P_{\alpha\beta}(t+t_0) \cdot P_{\alpha\beta}(t_0) \right\rangle dt \quad (2)$$

Here, the deviatoric stress tensor $P_{\alpha\beta}$, which is the symmetrized traceless portion of the stress tensor $\sigma_{\alpha\beta}$ computed at every FPMD (first-principles molecular dynamics) step, is defined as (Chen et al. 2009)

$$P_{\alpha\beta} = \frac{1}{2}(\sigma_{\alpha\beta} + \sigma_{\beta\alpha}) - \frac{1}{3}\delta_{\alpha\beta}\left(\sum_\lambda \sigma_{\lambda\lambda}\right) \quad (3)$$

where $\delta_{\alpha\beta}$ is the Kronecker δ. Using both the off-diagonal (with a weighting factor of 1) and diagonal (with a weighting factor 4/3) components improves the statistics (Chen et al. 2009; Nevins and Spera 2007).

The mean square displacement, MSD (in Eq. 1), and stress autocorrelation function, ACF (in Eq. 2), represented by angular brackets are averaged over different time origins, t_0 values (i.e., different initial configurations). Figure 1 shows the MSD and viscosity curves at different conditions. The diffusive (linear) regime (a slope of unity in the log-log MSD plot) and shear relaxations (the plateau in the viscosity or Green-Kubo integral) occur well within the simulation durations. At two conditions, namely 0.55V_X, 3000 K (51 GPa) and 0.45V_X, 4000 K (141 GPa), the liquid is in a deeply supercooled state showing very slow dynamics. The slowest moving species (Ca) reaches the maximum MSD of ~5 and ~4 Å^2, respectively, at these conditions. The linear regime does appear in the Ca MSD plot although it is delayed considerably. Also, the total MSD exceeds 10 Å^2 at both conditions. Because the statistics degrade toward the end of the simulation, it is better to make diffusivity and viscosity estimates at a time once the linear regime in the MSD curve or the plateau in the viscosity curve has been reached to avoid larger errors (Chen et al. 2009). Such optimal time varies from run to run but it tends to increase on cooling and compression. The uncertainty generally becomes larger at lower temperature and/or higher pressure with its typical values lying within 20 and 30% for the diffusivity and viscosity, respectively. These sizes are acceptable given that the transport properties vary exponentially with both temperature and pressure (i.e., they vary by two to three orders of magnitude over the pressure-temperature ranges studied here, see the results and discussion sections). The uncertainty, particularly in the case of viscosity, exceeds 50% as the liquid goes deeper in the supercooled state at highly compressed volumes (0.55V_X and 0.45V_X).

Simulation Results

First, we present the calculated pressure-volume-temperature results (Fig. 2), which can be accurately represented by the third-order Birch-Murnaghan equation of state (EOS) for the reference isotherm, $P(V,T_0)$, and a simple form of the thermal pressure, $P_{TH}(V,T) = B(V)(T - T_0)$. The 3000 K reference EOS parameters are: V_0 = 193 (±2) Å^3 per formula unit, K_0 = 11.5 (±3) GPa and K_0' = 6.8 (±6), and the thermal pressure coefficient is: $B(V) = 29.8 - 0.288V + 0.00073V^2$ in MPa/K. The calculated P-V isotherms gradually diverge on compression because the thermal pressure increases on compression. Further details on EOS and thermal properties of anorthite liquid can be found in de Koker (2010).

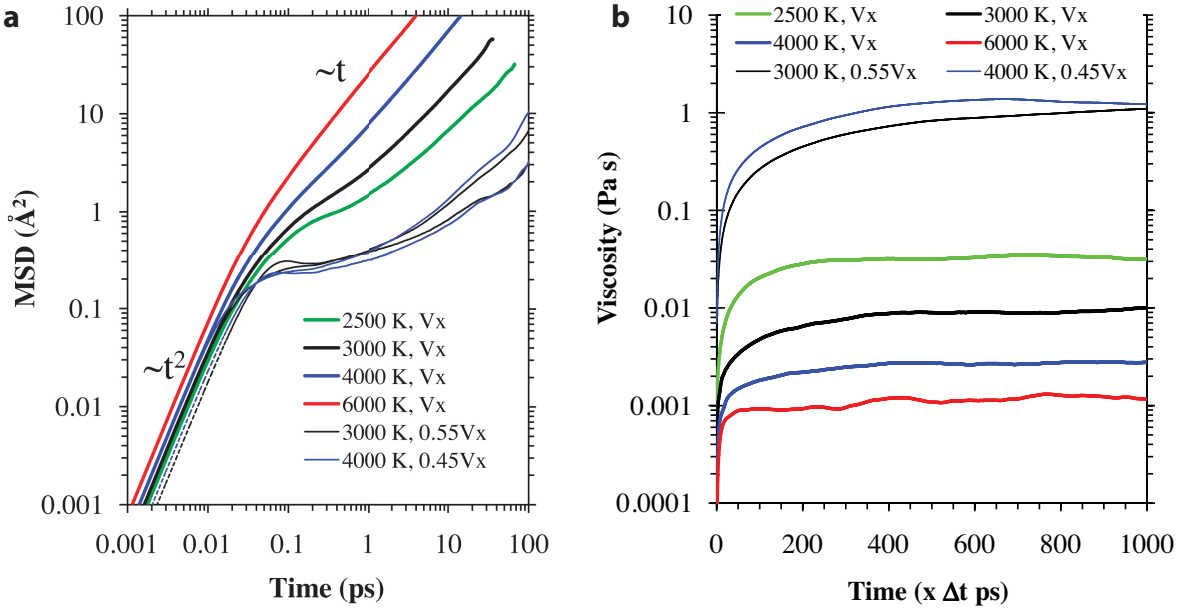

Figure 1. Total mean square displacement (MSD) and viscosity as a function of maximum time used in evaluating Equations 1 and 2. The MSD and viscosity curves are at different temperature and volume conditions as shown. The dotted lines represent the partial Ca MSD at 0.55V_X and 3000 K (upper), and 0.45V_X and 4000 K (lower). The value of Δt is 0.001, 0.002, 0.004, 0.02, 0.05, and 0.05 for viscosity curves from the bottom to the top. (Color online.)

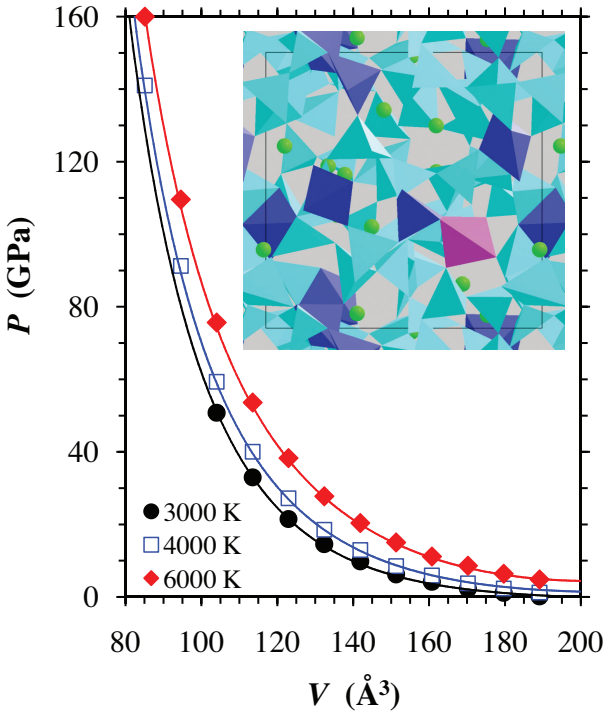

FIGURE 2. Calculated pressure-volume equation of state isotherms of anorthite liquid along 3000 K (circles), 4000 K (squares), and 6000 K (diamonds). The uncertainties are within the size of symbols used. The inset shows the liquid structure at the reference volume (3000 K, 0.2 GPa) consisting of mainly Si/Al-O tetrahedra (cyan), a few Al-O pentahedra (blue), and one Al-O octahedron (magenta), with Ca atoms (spheres) in the background. Color online.

TABLE 1. Arrhenius fit parameters for the temperature variations of self-diffusion coefficients and viscosity around 0 GPa of anorthite liquid

Parameters	D_{Ca}	D_{Al}	D_{Si}	D_O	η
D_0 (x 10^{-9} m^2/s) or η_0 (Pa·s)	710	1095	1290	1450	0.000015
E_D or E_η (kJ/mol)	117 (8)	149 (5)	166 (6)	158 (4)	162 (13)
E_D or E_η (kJ/mol)	172*		179†	174†	210‡, 275§

Note: The experimental data are for hyplobasaltic (* = La Tourrette et al. 1996), basaltic († = Lesher et al.1996), anorthitic (‡ = Urbain et al. 1982), and dacitic (§ = Tinker et al. 2004) melts.

TABLE 2. Ca-O, Al-O, Si-O bond related parameters at different conditions

V, T (K), P (GPa)	Ca-O		Al-O		Si-O	
	α_B	α_T	α_B	α_T	α_B	α_T
V_X, 3000, 0.2	417	0.14	211	0.24	48	0.39
V_X, 4000, 1.2	497	0.21	352	0.33	156	0.44
V_X, 6000, 4.8	680	0.35	680	0.46	472	0.50
$0.7V_X$, 3000, 15	494	0.17	317	0.21	119	0.30
$0.55V_X$, 3000, 51	539	0.04	463	0.06	272	0.07

Note: α_T represents the fraction of the bond events, which result in the formation of new bonds and thus cause the transfer of oxygen from one coordination shell to another. α_B is the rate of bond-breakings (per picosecond).

Self-diffusion coefficients

The calculated self-diffusion coefficients for all species increase with increasing temperature at zero pressure (Fig. 3a) closely following the Arrhenian relation: $D_\alpha = D_{0\alpha}\exp[-E_{D\alpha}/(RT)]$ where α represents Ca, Al, Si, and O. The activation energies fall in the range 117 to 166 kJ/mol (Table 1), which are generally smaller than the values derived from low-temperature (<2000 K) experimental data for silicate melts with similar bulk compositions.

Our results at 2500 K show that Ca is the fastest species, whereas Si is the slowest species with D_{Ca}/D_{Si} = 6.5. The predicted ordering of $D_{Ca} > D_{Al} \approx D_O > D_{Si}$ agrees with the measured ordering for the composition $20CaO\text{-}20Al_2O_3\text{-}60SiO_2$ (wt%) at 1 GPa and 1773 K (Liang et al. 1996). Note that anorthite is $20CaO\text{-}37Al_2O_3\text{-}43SiO_2$. Different diffusivities converge as temperature increases. Relatively small diffusion differences at high temperatures suggest that the mechanisms for all species are similar at high temperatures in that they involve flow-like motion of particles mediated by frequent bond breakings occurring at similar rates for all cation-anion bonds (Table 2). As temperature decreases, the mechanisms become increasingly sensitive to local structural environments and different species see different local potentials. In particular, a Si atom sits in deeper minima and its diffusion motion is not simply related to breakage of the bond with one of its oxygen neighbors. On the other hand Ca atoms, being relatively weakly bonded to O atoms compared to bonding between Si (or Al) and O atoms, can move easily in open space available at large volumes. Consistently, Mg was also predicted to be the fastest species in $MgSiO_3$ liquid (Karki et al. 2010). This is supported by the observation that the Ca-O and Mg-O bonds are much weaker than the Al-O and Si-O bonds, and hence are broken at much higher rates (Table 2).

The calculated self-diffusivities vary with pressure in a way that is sensitive to temperature (Fig. 4). At 6000 K, they show the normal trend that the diffusivity decreases monotonically with pressure. As temperature is decreased, the pressure dependence becomes stronger. At 3000 K, all framework ions (Al, Si, and O) show weak anomalous diffusion in the low-pressure regime—the diffusivities initially increase slowly or remain unchanged with pressure up to about 5 GPa. The diffusivities rapidly decrease on further compression, i.e., normal diffusion appears in the high-pressure regime. Such a change in the pressure behavior was predicted by previous MD studies of anorthite liquid (Nevins et al. 1998; Spera et al. 2009). Other silicate liquids, including silica liquid, also show anomalous diffusion as confirmed by recent first-principles simulations (Karki and Stixrude 2010b). In agreement with theory, low-pressure experiments have found that the diffusivity increases with pressure in polymerized silicate melts such as dacite (Tinker et al. 2003).

All three isotherms for diffusivity plotted in the logarithmic scale (i.e., $\log D_\alpha$) in Figure 4 are not straight lines suggesting that diffusivity does not vary with pressure according to the standard Arrhenian law. We represent the complicated pressure variation of diffusion coefficient for each species, α, using the modified Arrhenian relation:

$$D_\alpha(P,T) = \exp[-A(P) - \{B(P) - C(P)/T\}/(RT)] \quad (4)$$

where the parameters A, B, and C are defined in Table 3. This means that the activation volume, $V^*_{D\alpha} \propto (\partial \ln D_\alpha/\partial P)_T$, is a function of both pressure and temperature. The anomalous regime corresponds to negative (small) activation volumes at low pressures along 3000 K. The activation volumes become positive

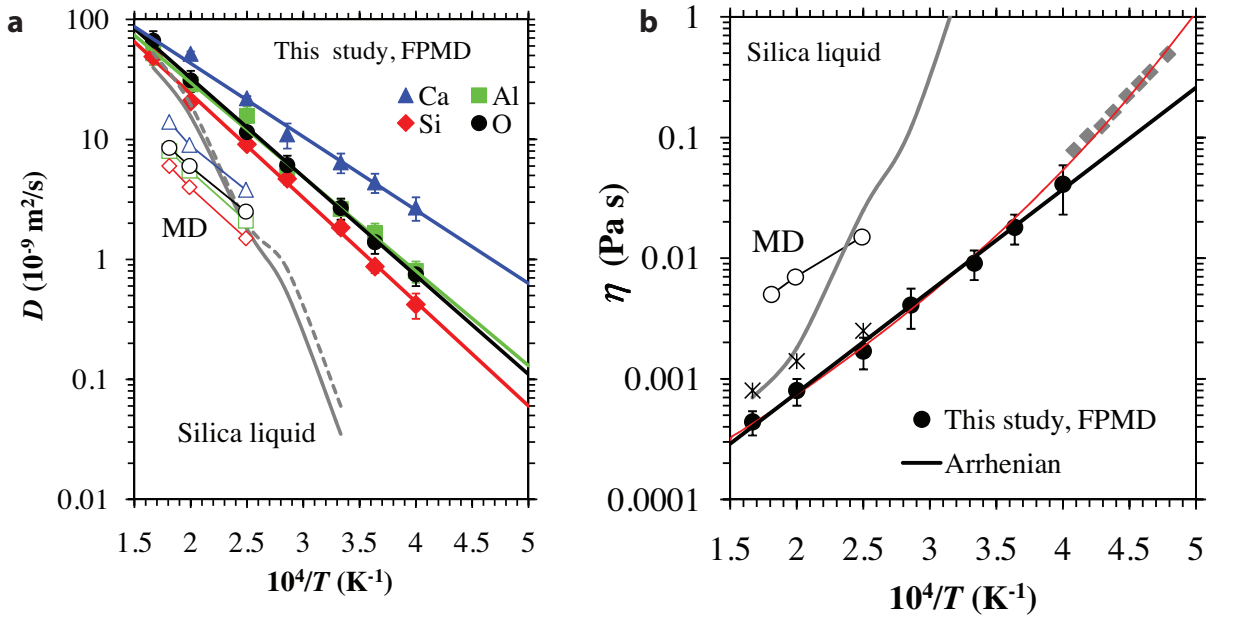

FIGURE 3. Calculated self-diffusivities of different species (**a**) and viscosity (**b**) at V_X (2500 K, 0.0 GPa), V_X (2750 K, 0.1 GPa), V_X (3000 K, 0.2 GPa), V_X (3500 K, 0.6 GPa), $1.14V_X$ (4000 K, 0.5 GPa), $1.26V_X$ (5000 K, 0.7 GPa), and $1.33V_X$ (6000 K, 1.1 GPa). The straight lines are the Arrhenian fits. Also shown is the VFT fit (red curve) to the viscosity results along with the experimental data (diamonds) from Urbain et al. (1982). The reference volume (V_X) results at 4000 K (1.2 GPa), 5000 K (2.7 GPa), and 6000 K (4.8 GPa) are shown (asterisks) only for the viscosity (the V_X diffusivities being consistently smaller than those at the larger volumes by about 15, 23, and 32%, respectively). Our results are compared with the previous MD calculations (open symbols) of anorthite liquid (Spera et al. 2009) and first-principles calculations (gray lines) for silica liquid (Karki and Stixrude 2010b). (Color online.)

FIGURE 4. Self-diffusion coefficients of Ca, Al, Si, and O in anorthite liquid as a function of pressure at 3000 K (circles), 4000 K (squares), and 6000 K (diamonds). The lines are fit to the modified Arrhenius relation (Eq. 4). The previous MD results (open squares) for anorthite liquid at 4000 K (Spera et al. 2009) and first-principles results (gray line) for silica liquid at 3000 K (Karki and Stixrude 2010b) are also shown for comparison. (Color online.)

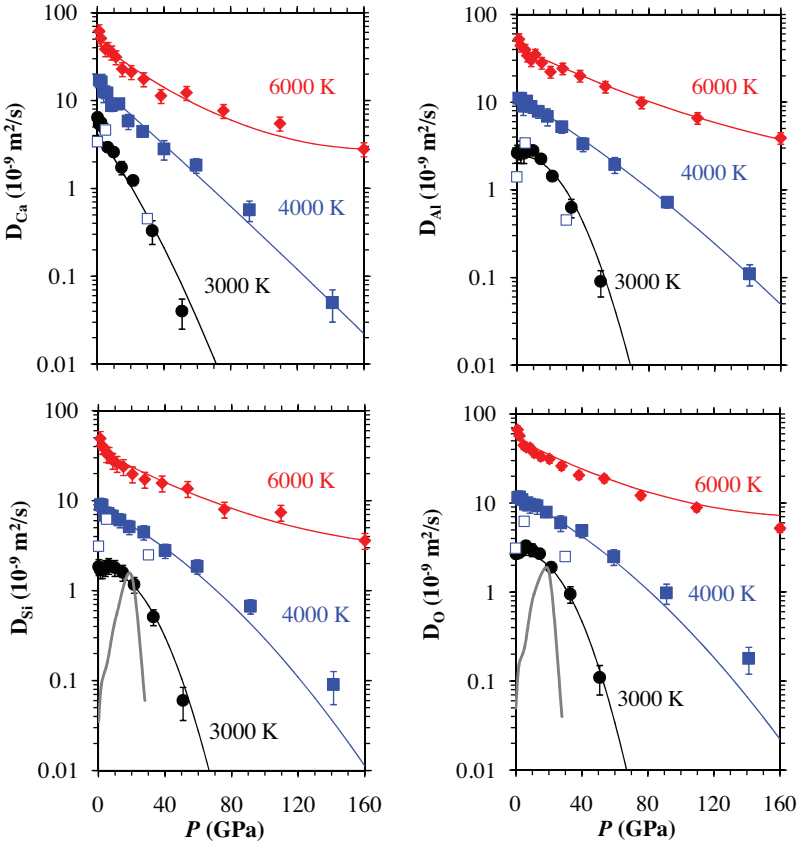

TABLE 3. Modified-Arrhenius fit parameters (Eqs. 4 and 5) for the pressure-temperature variations of self-diffusion coefficients and viscosity of anorthite liquid*

Parameters	D_{Ca}	D_{Al}	D_{Si}	D_O	η
A_0	−5.5	−5.6	−6.2	−6.8	−10.8
A_1	0.08	−0.11	−0.06	−0.09	0.02
A_2	0.00024	0.0032	0.0026	0.0032	0.0014
B_0/R	8108	7491	13715	16256	24568
B_1/R	−473	1261	851	1131	191
B_2/R	−4.3	−33	−28	−34	−16
C_0/R	12338511	19596458	10161126	4354768	−22215126
C_1/R	1299173	−2859631	−2112063	−2743504	−327043
C_2/R	13427	81563	72454	86592	43132

* $A(P) = A_0 + A_1P + A_2P^2$, $B(P) = B_0 + B_1P + B_2P^2$, and $C(P) = C_0 + C_1P + C_2P^2$.

when pressure and temperature increase to reach outside the anomalous regime. These changes are significant in that the diffusivity isotherms show change in their curvatures from concave to convex between 3000 and 6000 K. Such changes turn out to be robust features predicted in other liquids as well (Karki et al. 2010; Karki and Stixrude 2010a, 2010b).

Viscosity

The calculated viscosity decreases with increasing temperature at zero pressure (Fig. 3b). The Arrhenian representation ($\eta = \eta_0 \exp[E_\eta/(RT)]$) of viscosity over the range 2500 to 6000 K gives the activation energy 162 kJ/mol, which is lower than the experimentally derived values (≥200 kJ/mol) for anorthite liquid (Urbain et al. 1982) and other liquids (e.g., Tinker et al. 2004) (Table 1). Low-temperature extrapolation of the calculated viscosity results systematically deviates from the experimental data (Urbain et al. 1982). This suggests that the activation energy is a function of temperature, changing from a high value obtained from low-temperature measurements to a low value obtained from high-temperature simulations. The Vogel-Fulcher-Tammann (VFT) formulation, $\eta = A\exp[B/(T - T_0)]$, with A = 0.000038 Pa·s, B = 12200 K, and T_0 = 800 K) permits the activation energy to vary with temperature over a wide range in a way that is seen in other silicate melts (Karki and Stixrude 2010a) (see Fig. 3b).

As in the case of the diffusion, the pressure variation of the viscosity is sensitive to temperature and the logη curves are not straight lines (Fig. 5). We represent the complex P-T behavior by the modified Arrhenian relation:

$$\eta(P,T) = \exp\left[A(P) + \left\{ B(P) + C(P)/T \right\} / (RT) \right] \quad (5)$$

where the parameters A, B, and C are given in Table 3. Whereas the 6000 and 4000 K isotherms show normal trend of increasing viscosity on compression, the 3000 K isotherm shows a weak anomalous behavior—it initially decreases slightly with pressure, reaches the minimum around 5 GPa and increases at higher pressures. Accordingly, the activation volume, $V_\eta \propto (\partial \ln\eta / \partial P)_T$, is small negative at low pressures (<5 GPa) and 3000 K, whereas it is positive at all other pressure and temperature conditions. The viscosity isotherm changes from a convex curve to a concave curve between 3000 and 6000 K, which is opposite to the case of diffusion. The other liquids including $MgSiO_3$ (Karki and Stixrude 2010a) and SiO_2 (Karki and Stixrude 2010b) were predicted to show similar pressure-temperature behavior of the viscosity including the viscosity anomaly at 3000 K. Our prediction is also consistent with the low-pressure experimental observations of viscosity decreasing with pressure in polymerized silicate melts (Tinker et al. 2004; Behrens and Schulze 2003).

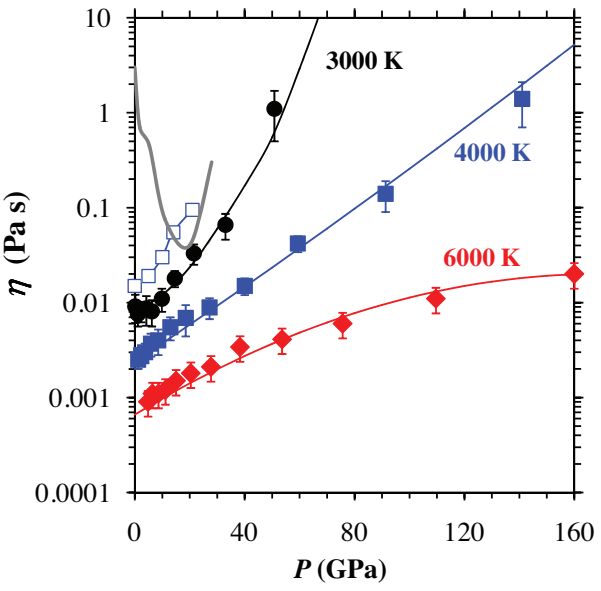

FIGURE 5. Pressure variations of viscosity (solid symbols) of anorthite liquid at 3000 K (circles), 4000 K (squares), and 6000 K (diamonds) fit to the modified Arrhenian relation (Eq. 5). The previous MD results (open squares) for anorthite liquid at 4000 K (Spera et al. 2009) and first-principles results (gray line) for silica liquid at 3000 K (Karki and Stixrude 2010b) are shown for comparison. (Color online.)

DISCUSSION

Diffusivity differences among different species are suppressed on compression: the D_{Ca}/D_O, D_{Al}/D_O, and D_{Si}/D_O ratios (along 3000 K) are 2.4, 1.0, and 0.7, respectively, at zero pressure and 0.3, 0.7, and 0.5, respectively, at high pressure (51 GPa). Calcium changes from being the fastest species at low pressure to the slowest species at high pressure, whereas Si is the slowest species at low pressure and oxygen is the fastest species at high pressure. Pressure-induced slowing down of Ca can be associated with the enhanced local structure consisting of Ca and O atoms. Note that the Ca-O radial distribution function (RDF) becomes sharper and taller closely resembling Al-O and Si-O RDFs, and that the Ca-O coordination tends to saturate with increasing pressure (Fig. 6). We also find that all three cation-anion bond-breaking rates become similar (Table 2). As such, all cations become systematically slower than the anion and their diffusion coefficients tend to be comparable with each other roughly following the atomic mass order ($m_{Ca} > m_{Si} > m_{Al}$).

Our calculated self-diffusion coefficients are expected to be superior to those from recent first-principles study (de Koker 2010), which used a smaller supercell (104 atoms) and shorter simulations (<10 ps). In particular, the differences between the two studies are important at lower temperatures and higher pressures, where longer runs are needed to achieve diffusive regime (where MSD is proportional to time). We also ensure that total

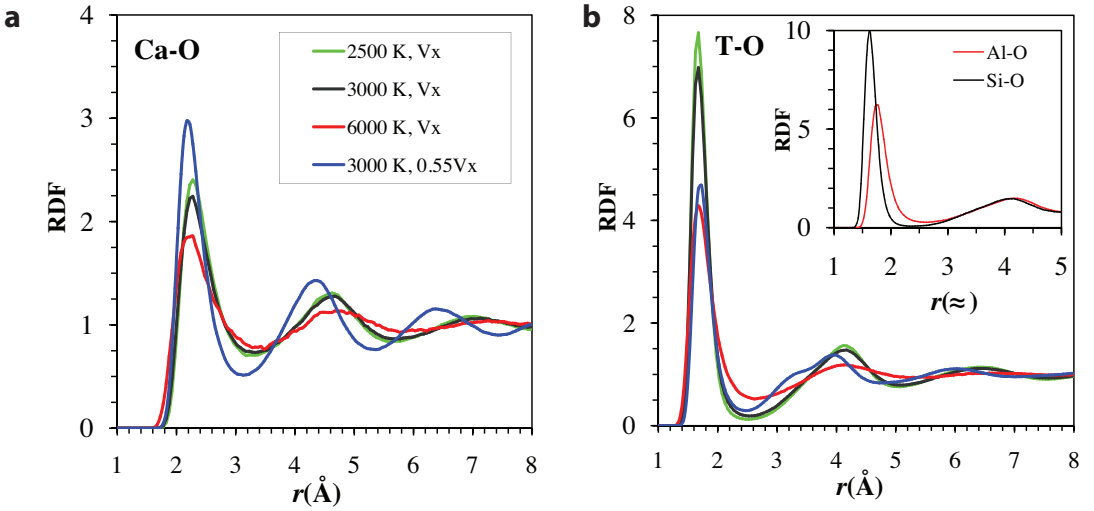

FIGURE 6. Ca-O (**a**) and T-O (**b**) (where T is Al/Si) radial distribution functions of anorthite liquid at different conditions shown. The inset shows the Al-O and Si-O components of T-O RDF at V_X and 3000 K. (Color online.)

MSD exceeds 10 Å^2 at each *P*-*T* condition studied. Although our results for both viscosity and diffusivities qualitatively agree with the previous pair-potentials MD calculations (Nevins and Spera 1998; Spera et al. 2009), the quantitative differences are large. Comparisons with the experimental data for the viscosity of anorthite liquid at zero pressure (Urbain et al. 1982) suggest that the pair-potential calculations most likely have overestimated the viscosity and, consistently, underestimated the diffusion coefficients. As mentioned earlier, the activation energies of diffusivity and viscosity (at zero pressure) predicted by the simulations (both first-principles and pair-potentials) tend to be consistently lower than their experimentally derived values for anorthite and other silicate liquids (Karki and Stixrude 2010a, 2010b; Spera et al. 2009; Nevins et al. 2009). Much of the difference can be attributed to a dependence of the activation energy on temperature as suggested by the VFT representation of our viscosity results (Fig. 3b).

Comparison with previous first-principles results of silica liquid (Karki and Stixrude 2010b) allows us to examine the effects of CaO and Al_2O_3 components on the dynamics of anorthite liquid in relation to the structural changes. We find that the Si and O self-diffusivities (viscosity) of silica liquid are smaller (larger) than the corresponding values of anorthite liquid by more than one order of magnitude at 3000 K (Fig. 3). Also, silica liquid shows a much stronger anomalous pressure behavior of diffusivity and viscosity (Figs. 4 and 5). Temperature suppresses the dynamical differences between two liquids. Both liquids are usually considered to be highly polymerized structures. The large dynamical differences can be attributed to the structural modifier content (Ca atom) of anorthite liquid, which breaks up polymerization as previously suggested (e.g., Giordano and Dingwell 2003; Giordano et al. 2006). Here, we further elaborate on why the anorthite liquid is so much more mobile than the silica liquid.

First, the structural polymerization of anorthite liquid consists of Al-O and Si-O bonds in almost equal numbers, whereas that of silica liquid consists of only Si-O bonds. We find the Al-O bonds to be larger and weaker than the Si-O bonds. The calculated Al-O RDF shows shorter and broader first peak located at larger distance, compared to the peak in the Si-O RDF (Fig. 6b). This is consistent with larger effective size of the Al ion. Our calculations also show that the Al-O bonds are broken more often than the Si-O bonds, as many as four times at 3000 K and V_X (Table 2).

Second, the odd coordination species are much more abundant in anorthite liquid than in silica liquid (Table 4). Non-bridging oxygen (NBO) and oxygen tri-clusters (O3) are present in large amounts (12% and 18%, respectively, at 3000 K and 0 GPa), compared to a total of 1% in silica liquid. Among the bridging oxygen, only one fourth connects two Si atoms, whereas all remaining also involve bonding with aluminum. Non-tetrahedral states consisting of three- and five-oxygen coordinated Si and Al atoms together account for more than 20% compared to less than 2% in silica liquid. It is increased proportions of odd coordination (NBO, O3, non-tetrahedral states) that systematically enhance the dynamics of anorthite liquid relative to that of silica liquid as explained below. Note that NBO, O3 and fivefold Al/Si have been detected experimentally in silicate melts and glasses (Stebbins and McMillan 1993; Stebbins and Xu 1997; Lee et al. 2004, 2008).

Non-bridging oxygen atoms contribute to the liquid dynamics at low pressures in two ways since it can be associated with the formation of both three- and five-coordinated T (Al or Si) atom. When one of two bonds of a BO with T atoms breaks, a

TABLE 4. Abundances of various T-O coordination species (denoted as $_ZC_{TO}$ and $_ZC_{OT}$) of anorthite and silica liquids

	$_3C_{TO}$	$_4C_{TO}$	$_5C_{TO}$	$_6C_{TO}$	$_0C_{OT}$	$_1C_{OT}$	$_2C_{OT}$	$_3C_{OT}$	$_4C_{OT}$
2500 K, 0 GPa	1.7	83	15	0.9	0.00	10	73	16	0.6
3000 K, ~0 GPa	3.0	76	19	2.0	0.04	12	69	18	0.8
silica	0.44	98	1.6	0.02	0.00	0.16	99	0.76	0.0
3000 K, ~5 GPa	0.87	52	39	7.8	0.00	7.4	61	30	2.5
silica	0.32	97	3.2	0.04	0.05	0.14	98	1.6	0.25
3000 K, ~20 GPa	0.07	12	45	39	0.00	2.3	40	47	10
silica	0.18	36	46	17	0.02	0.08	58	39	2.8
4000 K, ~2 GPa	8.6	62	26	3.4	0.04	14	62	22	1.7
silica	4.6	87	8.2	0.2	0.04	2.1	94	3.7	0.2
4000 K, ~140 GPa	0.00	0.05	4.8	55	0.00	1.2	15	49	32
silica	0.00	0.12	5.2	65	0.03	0.11	4.5	77	16

Note: Z represents the coordination number and T represents Al and/or Si.

tetrahedron (four-coordination) changes into a three-coordination state, which eventually forms bond with another O atom and turns back to a four-coordination state. On other hand, a NBO gets bonded to a four-coordinated silicon or aluminum to form a pentahedron (fivefold state), which eventually looses one of its original BOs as NBO and turns back into a tetrahedron. The bond breaking/formation events should not involve the same O atom (i.e., no recombination reactions) to make dynamical contribution. In effect, an oxygen atom thus exits from (enters into) and another oxygen atom enters into (exits from) the T coordination shell under consideration in the first (second) mechanism. These mechanisms (separately or in combination) are operative on initial compression where NBOs are highly abundant. The ratio $0.5({}_3C_{TO}/{}_1C_{OT})$ is small (<0.2) and decreases on compression (Table 4). This suggests that there are plenty of NBOs that can also participate in the pentahedral formation.

At pressures where pentahedral states become highly abundant (about 50%), NBOs are present in small amount (about 5%) but oxygen tri-clusters are present in a large amount (about 35%). Another way of forming pentahedron is that a BO gets bonded to a four-coordinated T atom and turns into O3. Suppose that a pentahedron (T_1) is formed when one BO atom (O_1) turns into O3. The O3 continues to exist and a second pentahedron (T_2) is formed by bonding to a BO atom (O_2) from the first pentahedron (T_1). Eventually, the T_1-O_2 and T_2-O_1 bonds break, and both O3s turn into BOs and both pentahdera turn into tetrahedra. The net result is thus an exchange of O atoms between two tetrahedra (T_1 and T_2). However, if the second pentahedron (T_2) is formed by bonding with a BO atom (O_3) from a third tetrahedron (T_3), then T_2-O_1 bond rupture results in a single oxygen atom transfer (i.e., O_1 from T_2 to T_1). The first pentahedron (T_1) and the second oxygen tricluster (O_3) continue to exist. Since the ratio $0.5({}_5C_{TO}/{}_3C_{OT})$ is high and increases on compression, this mechanism involving pentahedra and O3s is operative as the liquid is compressed.

Non-bridging oxygen and O3 coexisting in significant amounts complement each other to enhance the dynamical relevance of pentahedral states, whose abundance increases on compression. A pentahedral state is formed through NBO → BO or BO → O3 reaction capturing an oxygen atom, whereas it decays through BO → NBO or O3 → BO reaction releasing an oxygen atom. The importance of pentahedral states as an activated complex was previously proposed in the case of anorthite liquid (Spera et al. 2009) and other liquids (e.g., Kushiro 1978; Angell et al. 1982; Lesher et al. 1996; Behrens and Schulze 2003; Lee et al. 2004; Tinker et al. 2004; Karki and Stixrude 2010b).

Acknowledgments

This work was supported by NSF (EAR-0809489) and the U.K. National Environmental Research Council (NE/F01787/1). High-performance computational resources were provided by Louisiana State University (http://www.hpc.lsu.edu).

References cited

Angell, C.A., Cheeseman, P.A., and Tamaddon, S. (1982) Pressure enhancement of ion mobilities in liquid silicates from computer-simulation studies to 800-kilobars. Science, 218, 885–887.

Behrens, H. and Schulze, F. (2003) Pressure dependence of melt viscosity in the system $NaAlSi_3O_8$-$CaMgSi_2O_6$. American Mineralogist, 88, 1351–1363.

Bottinga, Y. and Richet, P. (1995) Silicate melts: The anomalous pressure dependence of the viscosity. Geochimica et Cosmochimica Acta, 59, 2725–2731.

Ceperley, D.M. and Alder, B.J. (1980) Ground state of the electron gas by a stochastic method. Physical Review Letters, 45, 566–569.

Chen, T., Smit, B., and Bell, A.T. (2009) Are pressure fluctuation-based equilibrium methods really worse than nonequilibrium methods for calculating viscosities? Journal of Chemical Physics, 131, 246101.

de Koker, N. (2010) Structure, thermodynamics and diffusion in $CaAl_2Si_2O_8$ liquid from first-principles molecular dynamics. Geochimica et Cosmochimica Acta, 74, 5657–5671.

de Koker, N., Stixrude, L., and Karki, B.B. (2008) Thermodynamics, structure, dynamics, and melting of Mg_2SiO_4 liquid at high pressure. Geochimica et Cosmochimica Acta, 72, 1427–1441.

Ghiorso, M.S. (2004) An equation of state for silicate melts. III. Analysis of stoichiometric liquids at elevated pressure: shock compression data, molecular dynamics simulations and mineral fusion curves. American Journal of Science, 304, 752–810.

Giordano, G. and Dingwell, D.B. (2003) Non-Arrhenian multicomponent melt viscosity: a model. Earth and Planetary Science Letters, 208, 337–349.

Giordano, D., Mangicapra, A., Potuzak, M., Russell, J.K., Romano, C., Dingwell, D.B., and Di Muro, A. (2006) An expanded non-Arrhenian model for silicate melt viscosity: A treatment for metaluminous, peraluminous and peralkaline melts. Chemical Geology, 229, 42–56.

Haggerty, S.E. and Sautter, V. (1990) Ultradeep (greater than 300 kilometers), ultramafic upper mantle xenoliths. Science, 248, 993–996.

Karki, B.B. and Stixrude, L. (2010a) Viscosity of $MgSiO_3$ liquid at Earth's mantle conditions: Implications for an early magma ocean. Science, 328, 740–743.

——— (2010b) First-principles study of enhancement of transport properties of silica melt by water. Physical Review Letters, 104, 215901.

Karki, B.B., Bhattarai, D., and Stixrude, L. (2006) First principles calculations of the structural, dynamical and electronic properties of liquid MgO. Physical Review B, 73, 174208.

——— (2007) First principles simulations of liquid silica: structural and dynamical behavior at high pressure. Physical Review B, 76, 104205.

Karki, B.B., Bhattarai, D., Mookherjee, M., and Stixrude, L. (2010) Visualization-based analysis of structural and dynamical properties of simulated hydrous silicate melt. Physics and Chemistry of Minerals, 37, 103–117.

Kresse, G. and Furthmuller, J. (1996) Efficiency of ab-initio total energy calculations for metals and semiconductors using a plane-wave basis set. Computational Materials Science, 6, 15–50.

Kresse, G. and Joubert, D. (1999) From ultrasoft pseudopotentials to the projector augmented-wave method. Physical Review B, 59, 1758–1775.

Kushiro, I. (1978) Viscosity and structural changes of albite ($NaAlSi_3O_8$) melt at high pressures. Earth and Planetary Science Letters, 41, 87–90.

La Tourrette, T., Wasserburg, G.J., and Fahey, A.J. (1996) Self diffusion of Mg, Ca, Ba, Nd, Yb, Ti, Zr and U in haplobasaltic melt. Geochimica et Cosmochimica Acta, 71, 1312–1323.

Lay, T., Garnero, E.J., and Williams, Q. (2004) Partial melting in a thermo-chemical boundary at the base of the mantle. Physics of Earth and Planetary Interiors, 146, 441–467.

Lee, S.K., Cody, G.D., Fei, Y., and Mysen, B.J. (2004) Nature of polymerization and properties of silicate melts and glasses at high pressure. Geochimica et Cosmochimica Acta, 68, 4189–4200.

Lee, S.K., Li, J.F., Cai, Y.Q., Hiraoka, N., Eng, P.J., Okuchi, T., Mao, H.K., Meng, Y., Hu, M.Y., Chow, P., and others. (2008) X-ray Raman scattering study of $MgSiO_3$ glass at high pressure: Implication for triclustered $MgSiO_3$ melt in Earth's mantle. Proceedings of the National Academy of Sciences, 105, 7925–7929.

Lesher, C.E., Hervig, R.L., and Tinker, D. (1996) Self-diffusion of network formers (silicon and oxygen) in naturally occurring basaltic liquid. Geochimica et Cosmochimica Acta, 60, 405–413.

Liang, Y., Richter, F.M., Davis, A.M., and Watson, E.B. (1996) Diffusion in silicate melts. I. Self-diffusion in CaO-Al_2O_3-SiO_2 at 1500 C and 1 GPa. Geochimica et Cosmochimica Acta, 60, 4353–4367.

Morgan, N.A. and Spera, F.J. (2001a) The glass transition, structural relaxation and theories of viscosity: a molecular dynamics study of $CaAl_2Si_2O_8$. Geochimica et Cosmochimica Acta, 65, 4019–4041.

——— (2001b) A molecular dynamics study of the glass transition in $CaAl_2Si_2O_8$: thermodynamics and tracer diffusion. American Mineralogist, 86, 915–926.

Nevins, D. and Spera, F. (1998) Molecular dynamics simulations of molten $CaAl_2Si_2O_8$: dependence of structure and properties on pressure. American Mineralogist, 83, 1220–1230.

——— (2007) Accurate computation of viscosity from equilibrium molecular dynamics simulations. Molecular Simulation, 33, 1261–1266.

Nevins, D., Spera, F.J., and Ghiorso, M.S. (2009) Shear viscosity and diffusion in liquid $MgSiO_3$: Transport properties and implications for terrestrial planet magma oceans. American Mineralogist, 94, 975–9801.

Revenaugh, J. and Sipkin, S.A. (1994) Seismic evidence for silicate melt atop the 410-km mantle discontinuity. Nature, 369, 474–476.

Rigden, S.M., Ahrens, T.J., and Stolper, E.M. (1984) Densities of liquid silicates

at high-pressures. Science, 226, 1071–1074.
Solomatov, V.S. (2007) Magma oceans and primordial mantle differentiation. In G. Schudbert, Ed., Treatise on Geophysics, vol. 9, p. 91. Elsevier, New York.
Spera, F.J., Nevins, D., Ghiorso, M., and Cutler, I. (2009) Structure, thermodynamic and transport properties of $CaAl_2Si_2O_8$ liquid. Part I: Molecular dynamics simulations. American Mineralogist, 73, 6918–6936.
Stebbins, J.F. and McMillan, P. (1993) Compositional and temperature effects on five-coordinated silicon in ambient pressure silicate glasses. Journal of Non-Crystalline Solids, 160, 116–125.
Stebbins, J. and Xu, Z. (1997) NMR evidence for excess non-bridging oxygen in an aluminosilicate glass. Nature, 390, 60–62.
Stixrude, L. and Karki, B.B. (2005) Structure and freezing of $MgSiO_3$ liquid in Earth's lower mantle. Science, 310, 297–299.
Taniguchi, H. (1992) Entropy dependence of viscosity and the glasstransition temperature of melts in the system diopside–anorthite. Contributions to Mineralogy and Petrology, 109, 295–303.
Tinker, D., Lesher, C.E., and Hutcheon, I.D. (2003) Self-diffusion of Si and O in diopside-anorthite melt at high pressure. Geochimica et Cosmochimica Acta, 67, 133–142.
Tinker, D., Lesher, C.E., Baxter, G.M., Uchida, T., and Wang, Y. (2004) High-pressure viscometry of polymerized silicate melts and limitations of the Eyring equation. American Mineralogist, 89, 1701–1708.
Urbain, G., Bottinga, Y., and Richet, P. (1982) Viscosity of liquid silica, silicates and alumino-silicates. Geochimica et Cosmochimica Acta, 46, 1061–1072.
Winkler, A., Horbach, J., Kob, W., and Binder, K. (2004) Structure and diffusion in amorphous aluminum silicate: A molecular dynamics study. Journal of Chemical Physics, 120, 384–393.

Manuscript received July 9, 2010
Manuscript accepted December 13, 2010
Manuscript handled by Charles Lesher